A multi-level uncertainty integration strategy for forward model-driven SHM

P. Gardner[1], **C. Lord**[1] **R. J. Barthorpe**[1]
[1] University of Sheffield, Department of Mechanical Engineering,
Mappin Street, Sheffield, UK, S1 3JD
e-mail: **pagardner1@sheffield.ac.uk**

Abstract
Conducting full-system testing can be costly and infeasible in many structural health monitoring (SHM) applications. In addition, many SHM methodologies require data from all likely damage scenarios in order to produce robust classifications. Forward model-driven SHM is an approach in which validated numerical models simulate full-system outputs under different damage scenarios, which are subsequently used as training data for machine learning methods, improving the problem of a lack of available data. Here a framework is proposed in which uncertainties characterised at a sub-system level, using sub-system experimental data, are integrated into full-system predictions. The proposed methodology for multi-level uncertainty integration seeks to propagate sub-system parameter uncertainties whilst inferring any model discrepancies at each level. This paper demonstrates the effectiveness of multi-level uncertainty integration for forward model-driven SHM on a numerical case study.

1 Introduction

Forward model-driven structural health monitoring (SHM) is the process by which computational models, (referred to as *simulators*) are utilised in a forward manner in order to generate damage features of a real world structure. Subsequently, the simulated damage features are used as training data for pattern recognition or machine learning techniques and decision bounds identified [1]. These approaches are useful as they seek to resolve problems with the lack of available damage state data common to most SHM applications. As a result, any forward model-driven strategy should not require damage state data at a full-system level (unless available) in order to resolve issues associated with data-driven approaches. As a consequence forward model-driven methods must employ a strategy that provides confidence in a full-system prediction without traditional validation at the full-system level. This provides the motivation for developing a multi-level uncertainty integration strategy.

Multi-level uncertainty integration is a process whereby a structure is divided into levels, where at the top is the full-system and below are potentially multiple levels of sub-systems, each with a number of simulators. For each sub-system it is expected that damage state data can be obtained, therefore allowing the simulators at this level to be calibrated and validated. The approach allows these sub-system models to feed into each other up until the full-system level. The key assumption is that uncertainty quantification can be adequately performed and understood at multiple sub-system levels and that all damage mechanisms of interest can be understood at a sub-system level.

This paper seeks to adapt a subfunction discrepancy approach used in health economics in order to gain confidence in whether to finance drug treatments [2]. The main idea is that model discrepancies, due to missing physics, approximations or assumptions, can be captured at each sub-system simulator and validated. These discrepancies are propagated through to the full-system level with each simulators' parameter uncertainties providing improved confidence in the full-system predictions and correcting simulator inadequacies.

The outline of this paper is as follows. Section 2 outlines the general approach to multi-level uncertainty integration and the importance of quantifying model discrepancy. A numerical case study is presented in Section 3 demonstrating the application of the multi-level uncertainty integration strategy. Finally, Section 4 states conclusions and further work.

2 Multi-Level Uncertainty Integration Strategy

Forward model-driven SHM relies on the ability to generate validated simulators of full-systems for various damage mechanisms of interest. A complication is that observational data for each of these damage states are not obtainable at a full-system level. This creates a problem in validating and gaining confidence in full-system simulators under damage, when observational data are often not available, motivating the development of a multi-level uncertainty integration strategy for forward model-driven SHM.

A multi-level uncertainty integration strategy uses a combination of validated sub-system simulators at various levels e.g. at material, component or sub-assembly level, in order to capture behaviours of the full-system, for which observational data cannot be obtained, with the aim of producing the required outputs under these behaviours. In an SHM context, the desired full-system outputs are damage sensitive features and the behaviours are generally the changes of these features under damage types of interest (although additional environmental changes may be included). Consequently, the method divides a full-system structure into a number sub-system simulators that meet certain requirements. Firstly, there must be an output that can be measured experimentally and used to validate the sub-system simulator for the required inputs $\boldsymbol{x}^{sub} \in \boldsymbol{x}^{full}$ (where the superscripts sub and $full$ indicate the sub-system and full-system levels). Secondly, it is imperative that the functional relationship contains a set of parameters $\boldsymbol{\theta}^{sub} \in \boldsymbol{\theta}^{full}$ and inputs $\boldsymbol{x}^{sub} \in \boldsymbol{x}^{full}$ that are included in or affect the full-system simulator. Accordingly, experimental data at each sub-system can be used to validate and make inferences about their respective simulator. Uncertainty quantification for each sub-system may be employed to quantify parameter, model discrepancy and observational uncertainties [3], leading to confidence in the sub-system simulator. These inferences can be propagated through to the next level of the strategy. A key assumption of a multi-level uncertainty integration strategy is that the physics controlling changes at a full-system level can be captured at multiple sub-system levels, in addition to corrections for model discrepancies and quantification of uncertainties. Once propagated to a full-system level, this results in a complete understanding of the full-system uncertainties and should reduce model form errors or missing physics to a negligible level for the desired output quantity.

The approach outlined in this paper adapts a subfunction discrepancy technique [2] in order to integrate uncertainties from sub to full-system level. The method in this paper relies on the use of each sub-system simulator being defined as a statistical model of the form presented in Eq. (1).

$$\boldsymbol{z}(\boldsymbol{x}) = \boldsymbol{y}(\boldsymbol{x}) + e = \eta(\boldsymbol{x}, \boldsymbol{\theta}) + \delta(\boldsymbol{x}) + e \tag{1}$$

Where $\boldsymbol{z}(\boldsymbol{x})$ and $\boldsymbol{y}(\boldsymbol{x})$ are observational and bias corrected simulator outputs given the inputs $\boldsymbol{x}$ respectively. The bias corrected simulator output is equal to the sum of the simulator $\eta(\boldsymbol{x}, \boldsymbol{\theta})$ and the model discrepancy $\delta(\boldsymbol{x})$, where $\boldsymbol{\theta}$ are parameters of the simulator. The observations are assumed to be uncertain reflected in the addition of e.

The subfunction method for the simplest case - one level, one sub-system simulator and one full-system simulator, where all the parameters are contained within the sub-system simulator - can be defined mathematically as in Eqs. (2) and (3).

$$\boldsymbol{y}^{sub}(\boldsymbol{x}) = \eta^{sub}(\boldsymbol{x}, \boldsymbol{\theta}) + \delta^{sub}(\boldsymbol{x}) \tag{2}$$

$$\boldsymbol{z}^{full} = \boldsymbol{y}^{full}(\boldsymbol{x}) + e^{full} = \eta^{full}(\boldsymbol{y}^{sub}(\boldsymbol{x}), \boldsymbol{\theta}) + e^{full} \tag{3}$$

In this case, by performing inferences and validating the sub-system level simulator using Eq. (2), confidence can be made in the outputs of the full-system model under the input $\boldsymbol{x}$. It is assumed in this example that model discrepancy is found only at the sub-system level. This means that the model discrepancy at a full-system is only dependent on that of the sub-system. It is noted that it is possible to add model discrepancy at a full-system level (Eq. (3)); this maybe useful for correcting non-input dependant model form errors.

Model discrepancy - the mismatch between simulator and observational data - can be formulated as several options. In Eq. (1) the model discrepancy is described as having a functional form, implying that the simulator does not include all physics and may have assumptions or approximations that affect the functional output. Considering a model discrepancy of this form is important for robust statistical inferences to be made [4]. In this paper a Gaussian Process (GP) regression model is utilised for inferring the functional form of the model discrepancy. GPs provide a Bayesian framework for inferring the functional mapping between inputs and outputs via a non-parametric formulation. Here a GP is used in order to map the simulator and observational data residuals. Accordingly, it is assumed that the residuals for different inputs are modelled as jointly Gaussian distribution. In order to preserve conciseness of this paper, the reader is referred to [5, 6] for more information on GPs.

3 Case Study

A numerical case study is presented as a demonstration of the multi-level uncertainty integration strategy from Section 2. The full-system is a linear four degree of freedom shear structure where each of the four masses is supported by a bolted beam Fig. 1a. The objective is to calculate the distributions of the four natural frequencies $\boldsymbol{\omega}_n = \{\omega_1, \omega_2, \omega_3, \omega_4\}$, as two damage types are introduced to the structure - an open crack of length l_{cr} at the midpoint of any of the four beams, and a reduction in the non-dimensionalised clamping force f, at any of the four bolted joints. For simplicity both damage types are assumed to only affect the stiffness K of the full-system and in a quasi-static manner where $K = (K_b \times K_j)/(K_b + K_j)$. Accordingly, the functional mapping of the full-system is defined as $X^{full} \rightarrow \boldsymbol{y}^{full}$ where $\boldsymbol{y}^{full} = \boldsymbol{\omega}_n$, $X^{full} = \{\boldsymbol{l_{cr}}, \boldsymbol{f}\}$ and the mapping depends on parameters $\boldsymbol{\theta}^{full}$. In addition, parameter distributions in this case study are fixed for both simulator and 'true' behaviours, stated in Table 1 (meaning that calibration is not pursued). The parameter distributions have been chosen so that a range of distributions are represented. Throughout the case study uncertainty propagation is performed via a Monte-Carlo approach using 500 draws from the parameter distributions in simulated cases. For experimental tests 50 repeats are performed, each repeat is an independent draw for the parameter distributions.

The first stage of a multi-level uncertainty integration strategy is to divide the full-system into corresponding sub-systems, for which there must be measurable outputs and either parameters or outputs that affect the full-system. This study divides the four degree of freedom shear structure by one level at which there are two sub-systems - the beam and bolted joint - presented in Fig. 1. The reason for this is that static deflection tests can be performed for an increase in damage in each sub-system, and subsequently, stiffness values can be determined from the experimental tests. Additionally, both sub-systems inform of the full-system response as each can be used to quantify the stiffness reduction under their respective damage type. The sub-systems can be defined as follows. For the beam sub-system (simulator one, level one): $\eta^{sub}_{1,1} : \boldsymbol{x}^{sub}_{1,1} \rightarrow \boldsymbol{y}^{sub}_{1,1}$ where $\boldsymbol{x}^{sub}_{1,1} = \boldsymbol{l}_{cr}$, and $\boldsymbol{y}^{sub}_{1,1} = \boldsymbol{K}_b$ the beam tip stiffness. For the joint sub-system (simulator two, level one): $\eta^{sub}_{2,1} : \boldsymbol{x}^{sub}_{2,1} \rightarrow \boldsymbol{y}^{sub}_{2,1}$ where $\boldsymbol{x}^{sub}_{2,1} = \boldsymbol{f}$, and $\boldsymbol{y}^{sub}_{2,1} = \boldsymbol{K}_j$ the joint stiffness. A full-system simulator is then formed as $\eta^{full} : \boldsymbol{x}^{full} \rightarrow \boldsymbol{y}^{full}$ for the inputs $X^{full} = \{\boldsymbol{n}_{cr}, \boldsymbol{n}_f, \boldsymbol{y}^{sub}_{1,1}(\boldsymbol{x}^{sub}_{1,1}), \boldsymbol{y}^{sub}_{2,1}(\boldsymbol{x}^{sub}_{2,1})\}$ and outputs $\boldsymbol{y}^{full} = \boldsymbol{\omega}_n$. The following subsections describe how each system is constructed with details on the simulator and numerical experimental data.

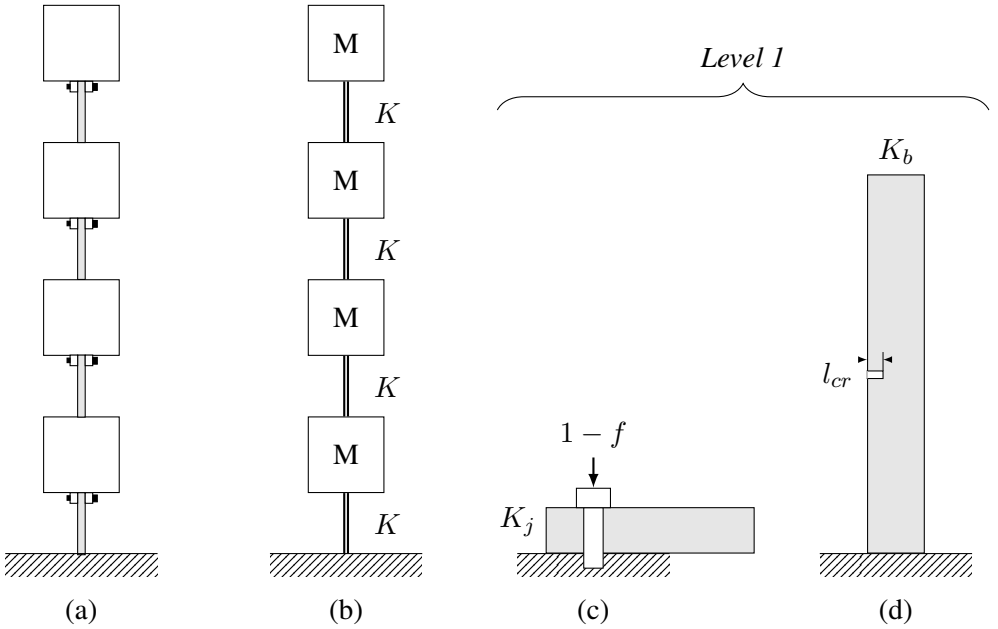

Figure 1: Schematics of the four degree of freedom shear structure; where (a) is the 'true' full-system with beams bolted to the underside of each plate, (b) is the full-system simulator where M is the mass of the blocks and K is the stiffness (a combination of the bolt and beam stiffness in series), (c) is the bolted joint sub-system for a reduction in the non-dimensionalised clamping force f, and (d) is the cantilever beam sub-system with a crack of length $\boldsymbol{l}_{cr}$.

3.1 Beam Sub-system

The four stiffness values K from the full-system are affected by the tip stiffness of a cantilever beam K_b. In this case study any of the four beams can be damaged by a midpoint crack x_{cr}, of increasing crack length l_{cr}, as depicted in Fig. 1d. In order to illustrate the fact that 'All models are wrong but some are useful' [7] - due to missing physics and/or approximations - the 'true' behaviour and the simulator are derived from different numerical models in the literature. The 'true' behaviour for the change in stiffness from an open crack is

Parameter		Value	System	'True'	Simulator
Beam length	l_b	$175mm$	$sub_{1,1}$, $full$	✓	✓
Beam width	w_b	$25mm$	$sub_{1,1}$, $full$	✓	✓
Beam thickness	t_b	$5mm$	$sub_{1,1}$, $full$	✓	✓
Plate length	l_p	$300mm$	$full$	✓	✓
Plate width	w_p	$250mm$	$full$	✓	✓
Plate thickness	t_p	$25mm$	$full$	✓	✓
Elastic Modulus	E	$\mathcal{N}\left(71, 0.5^2\right) GPa$	$sub_{1,1}$, $full$	✓	✓
Density	ρ	$\mathcal{N}\left(2700, 100^2\right) kg/m^3$	$full$	✓	✓
Beam length crack location	x_{cr}	$87.5mm$	$sub_{1,1}$	✓	✓
Crack model parameter	α	0.667	$sub_{1,1}$	✓	
Initial joint stiffness	K_{ji}	$\mathcal{W}ei\left(50005, 100\right) N/m$	$sub_{1,2}$, $full$	✓	✓
Rate of joint stiffness change	κ	$\mathcal{U}\left(4.9, 5.1\right)$	$sub_{1,2}$	✓	
Joint stiffness magnitude at $f=1$	p	$\mathcal{U}\left(1.99, 2.01\right)$	$sub_{1,2}$	✓	✓
Linear joint model gradient	β	$\mathcal{U}\left(-1.72, -1.68\right)$	$sub_{1,2}$		✓

Table 1: Parameters of the four degree of freedom shear structure. The 'true' and simulator columns refer to which numerical models the parameters are used in.

formulated using the numerical model defined by Christides and Barr [8] in Eq. (4). A bilinear stiffness model, by Sinha et al [9], forms the simulator, presented in Eq. (5). Both stiffness models are solved using the Euler-Bernoulli bending beam equation in Eq. (6) via numerical integration, where the beam stiffness is calculated via $K_b = -F/y_{tip}$ (y_{tip}[1] is the tip deflection). This means that both the 'true' behaviour and simulator for the beam sub-system map $\boldsymbol{l}_{cr} \rightarrow \boldsymbol{K}_b$. The simulator for this sub-system is the first simulator at level one - denoted $\eta^{sub}_{1,1}$.

$$EI(x) = \frac{EI_0}{1 + C\exp(-2\alpha|x - x_{cr}|/t_b)} \tag{4}$$

$$EI(x) = \begin{cases} EI_0 & \text{if } x \leq x_{cr,1} \text{ or } x \geq x_{cr,2} \\ EI_0 - E(I_0 - I_c)\frac{x - x_{cr,1}}{x_{cr} - x_{cr,1}} & \text{if } x_{cr,1} \leq x \leq x_{cr} \\ EI_0 - E(I_0 - I_c)\frac{x_{cr,2} - x}{x_{cr,2} - x_{cr}} & \text{if } x_{cr} \leq x \leq x_{cr,2} \end{cases} \tag{5}$$

$$\frac{\partial^2 y}{\partial x^2} = -\frac{M(x)}{EI(x)} \tag{6}$$

Where E is the elastic modulus, x is the distance along the length of the beam and M the bending moment. The second moment of areas $I_0 = (w_b t_b^3)/12$ and $I_0 = w_b(t_b - l_{cr})^3/12$ contribute to the constant $C = (I_0 - I_c)/Ic$, where w_t and t_b are the beam width and thickness respectively. The parameter α is set according to experimental work performed by Christides and Barr [8]. In the bilinear model positions beside the crack are calculated by $x_{cr,1} = x_{cr} - l_{eff}$ and $x_{cr,2} = x_{cr} + l_{eff}$ where the effective length of the stiffness reduction of the crack is $l_{eff} = 1.5t_b$, as defined by Sinha et al. [9].

The experiment for this sub-system is a static deflection test, due to the quasi-static assumptions in Eqs. (4) and (5). The beam was forced from $\boldsymbol{F} = \{100, 150, ..., 500\}N$ for each crack length $\boldsymbol{l}_c = \{0, 0.1, ..., 0.9\} \times t_b mm$ and the tip deflection $\boldsymbol{y}_{tip}$ measured (numerically using Eqs. (4) and (6)) with observational uncertainty distributed $\mathcal{N}\left(0, 1^2\right) mm$ $(= e^{sub}_{1,1})$. The experimental beam stiffness at the tip, was subsequently estimated via the gradient from least squares linear regression between the force and tip deflection.

The statistical equation in the form of Eq. (1) can be formulated as in Eq. (7).

$$\boldsymbol{z}^{sub}_{1,1}(\boldsymbol{x}^{sub}_{1,1}) = \eta^{sub}_{1,1}(\boldsymbol{x}^{sub}_{1,1}, \boldsymbol{\theta}^{sub}_{1,1}) + \delta^{sub}_{1,1}(\boldsymbol{x}^{sub}_{1,1}) + e^{sub}_{1,1} \tag{7}$$

Where $\boldsymbol{z}^{sub}_{1,1}(\boldsymbol{x}^{sub}_{1,1}) = \boldsymbol{K}^{exp}_b(\boldsymbol{l}_{cr})$ (the experimental beam tip stiffness), $\boldsymbol{x}^{sub}_{1,1} = \boldsymbol{l}_{cr}$. The bilinear numerical model forms the simulator $\eta^{sub}_{1,1}(\boldsymbol{x}^{sub}_{1,1}, \boldsymbol{\theta}^{sub}_{1,1})$, where $\boldsymbol{\theta}^{sub}_{1,1} = \{l_b, w_b, t_b, E, x_{cr}\}$ and the output is $\boldsymbol{y}^{sub}_{1,1}(\boldsymbol{x}^{sub}_{1,1}) = \boldsymbol{K}_b(\boldsymbol{l}_{cr})$. Both the observational uncertainty $e^{sub}_{1,1}$ and model discrepancy $\delta^{sub}_{1,1}(\boldsymbol{x}^{sub}_{1,1})$ are assumed unknown. Consequently, a GP regression model is utilised to infer both the model discrepancy and observational noise, regressing from crack lengths $\boldsymbol{l}_{cr}$ to the residual stiffness $\Delta\boldsymbol{K}_b = \boldsymbol{K}^{exp}_b - \boldsymbol{K}^{mode}_b$ where $mode$ indicates the simulator output at the modal values of the parameter distributions. Initially a leave-one-out validation process was used, where the 50 samples for each crack length were omitted periodically in training. However very little changes in the functional form were witnessed, leading to the full experimental data set being used in training. The bias corrected beam tip stiffness is compared to the simulator output and the experimental results in Fig. 2. This demonstrates the ability of a GP regression model to capture the functional form of the discrepancy whilst estimating a homoscedastic observational uncertainty (the results may be improved with a hetroscedastic observational uncertainty model in the GP regression model [10], this is left as an area for further research). The normalised mean squared error (NMSE) between the bias corrected and experimental data means are 0.097. showing good agreement.

[1]The notation y here indicates the deflection and not an output.

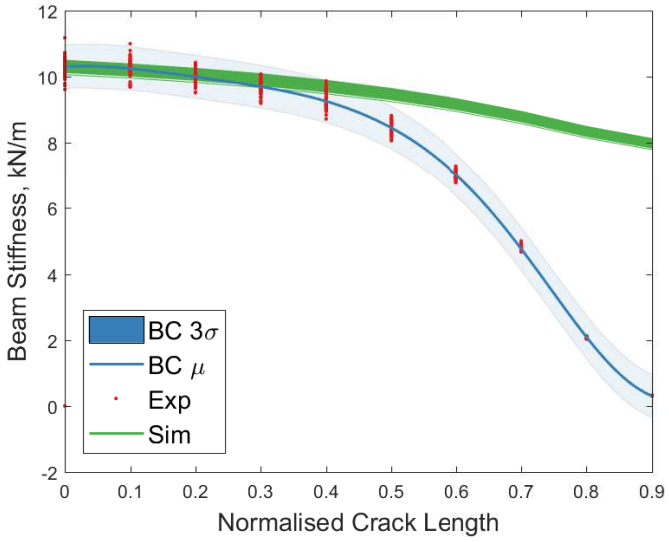

Figure 2: Comparison bias corrected (BC), experimental (exp) and simulator (sim) beam tip stiffness $\boldsymbol{K}_b$ for different crack lengths $\boldsymbol{l}_{cr}$.

3.2 Bolted Joint Sub-system

The bolted joint stiffness $\boldsymbol{K}_j$ at any of the four locations in the full-system can be damaged via a reduction in the clamping force, parametrised by a non-dimensional clamping force $\boldsymbol{f}$, presented in Fig. 1c. The 'true' behaviour and simulator output of $\boldsymbol{K}_j$, for a reduction in $\boldsymbol{f}$, are modelled numerically as shown in Eqs. (8) and (9) respectively; where Eq. (8) is a quasi-static bolt loosening model defined by Todd et al. [11, 12] and Eq. (9) is a linear fit of that numerical model. Consequently, the bolted joint sub-system maps $\boldsymbol{f} \rightarrow \boldsymbol{K}_j$. The simulator for this sub-system is the second simulator at level one - denoted $\eta^{sub}_{1,2}$.

$$K_j(f) = K_{ji} \times \tanh\left(\kappa(1-f)\right)\left(p + (1-p)\tanh\left(\kappa\frac{f}{1-f}\right)\right) \tag{8}$$

$$K_j(f) = K_{ji} \times (\beta f + p) \tag{9}$$

Where K_{ij} is the initial stiffness of the bolted joint, κ adjusts the rate of stiffness change, p adjusts the stiffness function magnitude at $f = 1$ and β is the gradient of the linear model. It is noted that the stiffness function is maximum at $f = 1$ and minimum and $f = 0$ to correspond with a reduction in force, meaning that the outputs for $\boldsymbol{f}$ are reversed.

The experiment for this sub-system is also static deflection test, due to the quasi-static assumptions in Eqs. (8) and (9). The beam was forced from $\boldsymbol{F} = \{100, 150, ..., 500\}N$ for each reduction in non-dimensionalised clamping force $\boldsymbol{f} = \{1, 0.9, ..., 0.1\}$ and the tip deflection measured (using Hooke's law $F = -K_j y$) with observational uncertainty distributed $\mathcal{N}\left(0, 1^2\right) mm$ $(= e^{sub}_{2,1})$. Again the experimental joint stiffness is estimated from the gradient of a least squares linear regression model.

The statistical equation in the form of Eq. (1) can be formulated as in Eq. (10).

$$\boldsymbol{z}^{sub}_{2,1}(\boldsymbol{x}^{sub}_{2,1}) = \eta^{sub}_{2,1}(\boldsymbol{x}^{sub}_{2,1}, \boldsymbol{\theta}^{sub}_{2,1}) + \delta^{sub}_{2,1}(\boldsymbol{x}^{sub}_{2,1}) + e^{sub}_{2,1} \tag{10}$$

Where $\boldsymbol{z}^{sub}_{2,1}(\boldsymbol{x}^{sub}_{2,1}) = \boldsymbol{K}^{exp}_j(\boldsymbol{f})$ (the experimental joint stiffness), $\boldsymbol{x}^{sub}_{2,1} = \boldsymbol{f}$. The simulator $\eta^{s}ub_{2,1}(\boldsymbol{x}^{sub}_{2,1}, \boldsymbol{\theta}^{sub}_{2,1})$, is linear numerical model (Eq. (8)) where $\boldsymbol{\theta}^{sub}_{2,1} = \{p, \beta, K_{ji}\}$ and the output is $\boldsymbol{y}^{sub}_{2,1}(\boldsymbol{x}^{sub}_{2,1}) = \boldsymbol{K}_j(\boldsymbol{f})$. Using a GP regression model, both the observational uncertainty $e^{sub}_{2,1}$ and model discrepancy $\delta^{sub}_{2,1}(\boldsymbol{x}^{sub}_{2,1})$ are

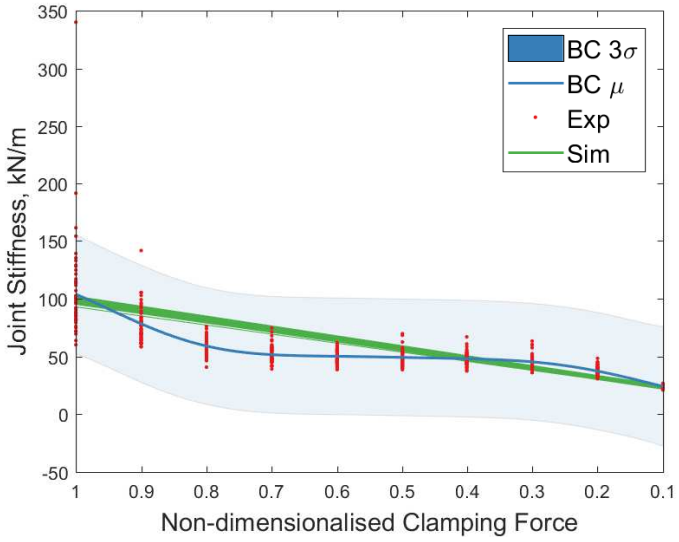

Figure 3: Comparison of bias corrected (BC), experimental (exp) and simulator (sim) joint stiffness $\boldsymbol{K}_j$ for a reduction in non-dimensionalised clamping force $\boldsymbol{f}$ - it is noted that the axis is reversed as [11, 12].

inferred in the same manner to the beam sub-system, regressing between $\boldsymbol{f}$ and $\Delta\boldsymbol{K}_j = \boldsymbol{K}_j^{exp} - \boldsymbol{K}_j^{mode}$. Similarly to the beam sub-system an initial leave-one-out validation process was employed, and due to relatively small changes in the functional form the full experimental data set was used in training. Fig. 3 shows a comparison for the bias corrected, simulator and experimental joint stiffness for a reduction in clamping force. As with the beam-subsystem, the bias corrected joint stiffness captures the functional form of the model discrepancy, which is not captured by the simulator. Homoscedastic assumptions in the GP regression model again mean that a homoscedastic observational uncertainty is inferred. The NMSE between the bias corrected and experimental data means are 0.001 showing excellent agreement.

3.3 Full-System Integration

The full-system is an undamped linear spring-mass system (Fig. 1b) where the spring stiffnesses K, are composed of the beam tip stiffness and bolt stiffness in series $K = (K_b \times K_j)/(K_b + K_j)$. The four degree of freedom system can be solved via an eigenvalue problem for the natural frequencies of the system. For this case study the 'true' and simulator numerical models are equivalent with the only difference being the input values for the beam tip and joint stiffnesses under damage. This means that there is no model discrepancy at the full-system level resulting in Eq. (11); due to the assumption that all the model discrepancy due to damage can be captured at a sub-system level. The percentage difference of natural frequency $\Delta\boldsymbol{\omega}_n$ is used as a damage feature in this case study, as it is a more damage sensitive feature compared to natural frequency [13].

$$\boldsymbol{z}^{full}(X^{full}) = \eta^{full}(X^{full}, \boldsymbol{\theta}^{full}) + e^{full} \tag{11}$$

Where $\boldsymbol{z}^{full}(X^{full}) = \Delta\boldsymbol{\omega}_n(X^{full})$, the percentage differences of the experimental four natural frequencies under damage. There are several inputs to the full-system $X^{full} = \{\boldsymbol{n}_{cr}, \boldsymbol{n}_f, \boldsymbol{y}_{1,1}^{sub}(\boldsymbol{x}_{1,1}^{sub}), \boldsymbol{y}_{2,1}^{sub}(\boldsymbol{x}_{2,1}^{sub})\}$ where $\boldsymbol{n}_{cr}$ and $\boldsymbol{n}_f$ indicate the floor in which the damage occurs, for the crack and loosened bolt respectively. As $\boldsymbol{n}_{cr}$ and $\boldsymbol{n}_f$ are only position inputs for this simple system it is assumed there no input dependent model discrepancy term is required. The other inputs are $\boldsymbol{y}_{1,1}^{sub}(\boldsymbol{x}_{1,1}^{sub}) = \boldsymbol{K}_b(\boldsymbol{l}_{cr})$, - the beam tip stiffness under a midpoint crack - $\boldsymbol{y}_{2,1}^{sub}(\boldsymbol{x}_{2,1}^{sub}) = \boldsymbol{K}_j(\boldsymbol{f})$, - the joint stiffness from a reduction in clamping force (dependent on their sub-system model discrepancy). The full-system simulator $\eta^{full}(X^{full}, \boldsymbol{\theta}^{full})$ also depends on the

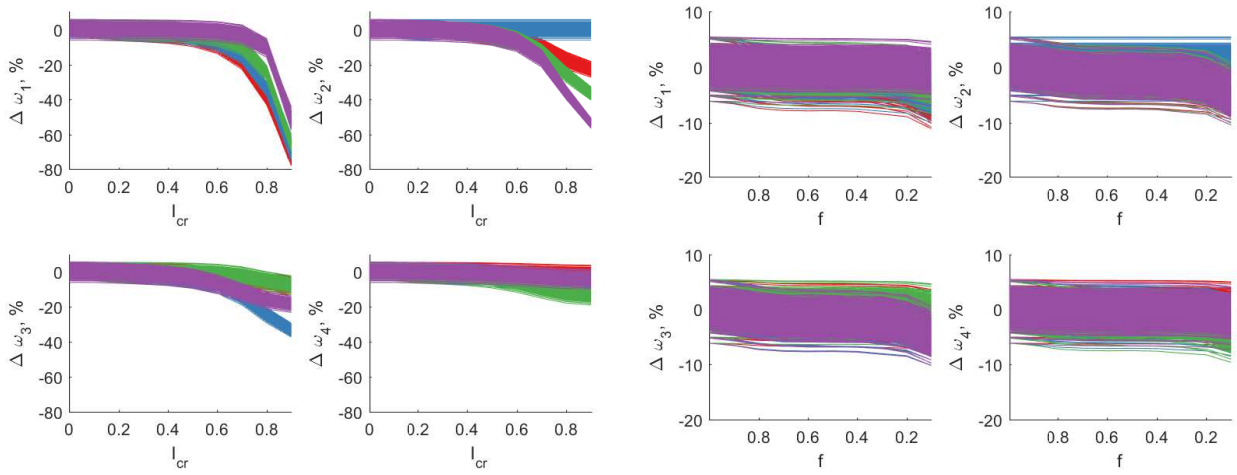

Figure 4: Bias corrected outputs - the percentage difference of the four natural frequencies $\Delta\boldsymbol{\omega}_n$ - for damage at different floors of the full-system $\boldsymbol{n}_{cr} = \boldsymbol{n}_f = \{1, 2, 3, 4\}$ (red, blue, green, purple); where (a) is an increase in crack length at the midpoint $\boldsymbol{l}_{cr}$ and (b) is a reduction in the non-dimensionalised clamping force $\boldsymbol{f}$. For (b) it is noted that the x-axis is reversed as [11, 12].

parameter set $\boldsymbol{\theta}^{full} = \{l_b, w_b, t_b, l_p, w_p, t_p, E, \rho, K_{ij}\}$. The numerical nature of this case study allows the comparison of both 'true' and simulator outputs, $\Delta\boldsymbol{\omega}_n$, under these damage types.

500 Monte Carlo realisations, drawn from the outputs of level one and the full system parameters, were generated in order to compare the bias corrected, simulator and 'true' full-system outputs. Figure 4 presents the bias corrected $\Delta\boldsymbol{\omega}_n$ under increasing crack length and for a reduction in clamping force. As expected, the increase in crack length has a greater effect on the natural frequencies of the system compared to a reduction in clamping force (reflected in the stiffness reductions in Figs. 2 and 3). The first natural frequency is the most affected by an increase in crack length, with a comparable reductions in the first, second and third natural frequencies for a reduction in clamping force. Figure 5 demonstrates an example comparison of the output distributions for $\Delta\omega_1$, where both damage types are located at the first floor and the only damage type is an increase in crack length. A visual comparison shows that for the first four damage states $\boldsymbol{l}_{cr} = \{0, 0.1, 0.2, 0.4\} \times t_b$, the distributions are very similar, after which the simulator fails to capture the correct distribution forms, whereas the bias corrected simulator maintains a good fit.

Hypothesis testing using the Kolmogorov-Smirnoff two sample test were performed at each damage scenario, for each natural frequency, totalling to 6400 combinations. A significance level, the upper bound of the probability of type 1 errors, was $\alpha_H = 0.01$. The percentage of null hypotheses H_0, that were not rejected, for both the bias corrected and simulator outputs at a full-system level, when compared to the 'true' outputs, were 97.4% and 30.7%. This demonstrates that the proposed uncertainty integration strategy outperforms an approach that does not consider model discrepancy, providing a significant improvement. In order to illustrate this further Fig. 6 presents a comparison between the uncertainty integration strategy and the original simulator for the first natural frequency; this was the worst performance of the uncertainty integration strategy. It can be seen that the performance of the uncertainty integration strategy is the same for all locations at 90% (in other natural frequencies there are differences at different locations). The original simulator however, performs best when damage is located at the highest floors, at 57%. This is because as damage is located at a lower floor it will have a greater affect on the first natural frequency of the system (as it is the first bending mode). Damage due to a crack located at the lower floors also affects the first natural frequency more than damage at the joint. This is expected from Figs. 2 and 3; both indicate the original simulator fails to capture the stiffness reduction for a crack to a greater extent than the due to a loosened bolt. The NMSEs for all 6400 combinations for both the original simulator and uncertainty integration strategy were 104 and

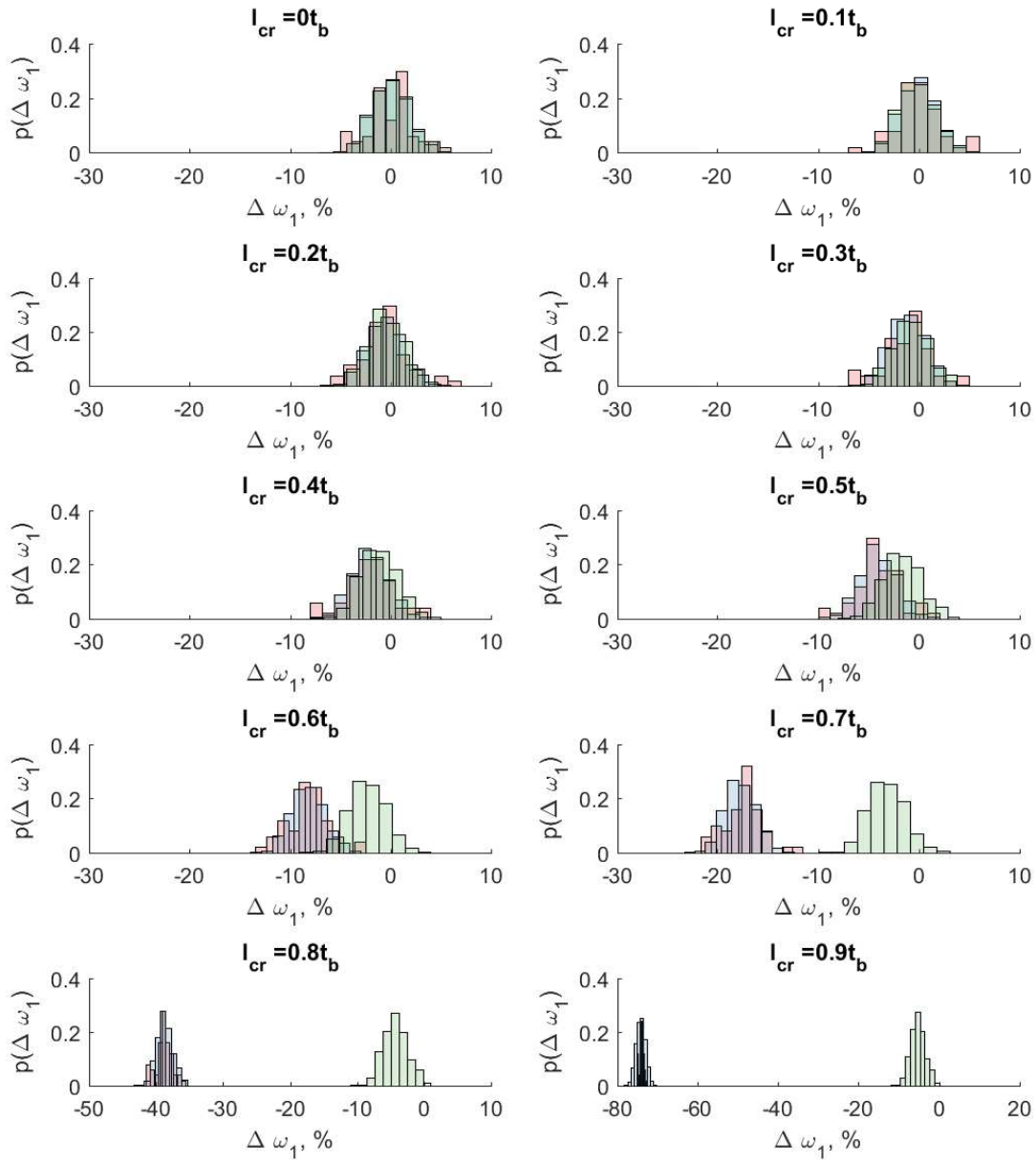

Figure 5: A comparison of $\Delta\boldsymbol{\omega}_1$ for increasing crack lengths at the midpoint of floor one; original simulator (green), uncertainty integration strategy (blue) and 'true' (red) outputs. It is noted that the axis limits are different for $\boldsymbol{l}_{cr} = \{0.8, 0.9\} \times t_b$ due to the large decrease in natural frequency.

0.005 respectively. This highlights the inability to capture the mean trend in the original simulator and the excellent agreement in the mean outputs for the uncertainty integration strategy and 'true' full-system.

In order to analyse these results further Fig. 7, a comparison of hypothesis test outcomes from all combinations of damage located at floor one, for the first natural frequency, are presented. This is chosen as the original simulator performs worse at this location, aiding the diagnoses of the difference in performance. The null hypothesis is rejected for all clamping force reductions when the crack length is at 90% of the beam

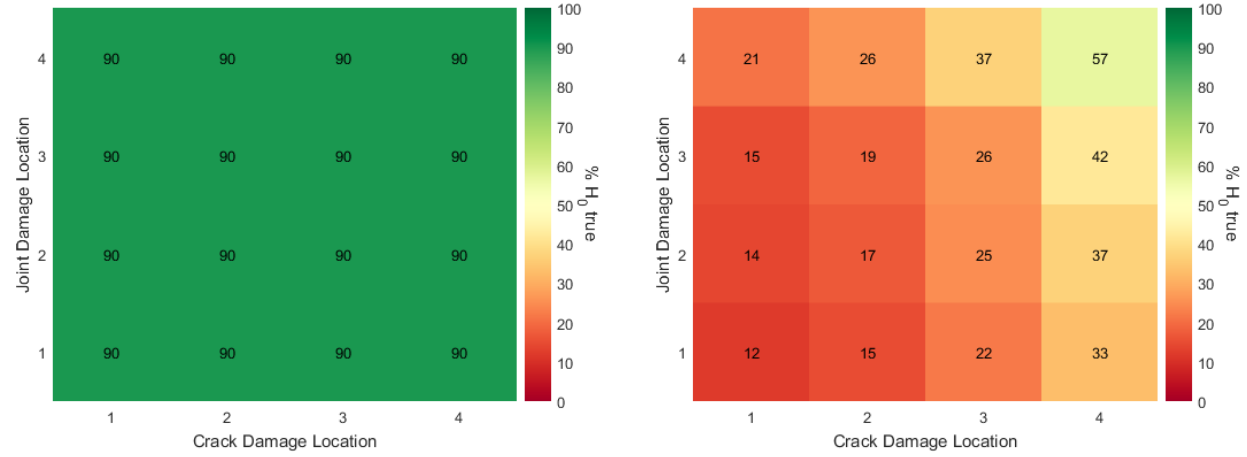

Figure 6: The percentage of null hypotheses H_0, that are not rejected for the first natural frequency; where (a) is the uncertainty integration strategy and (b) the original simulator.

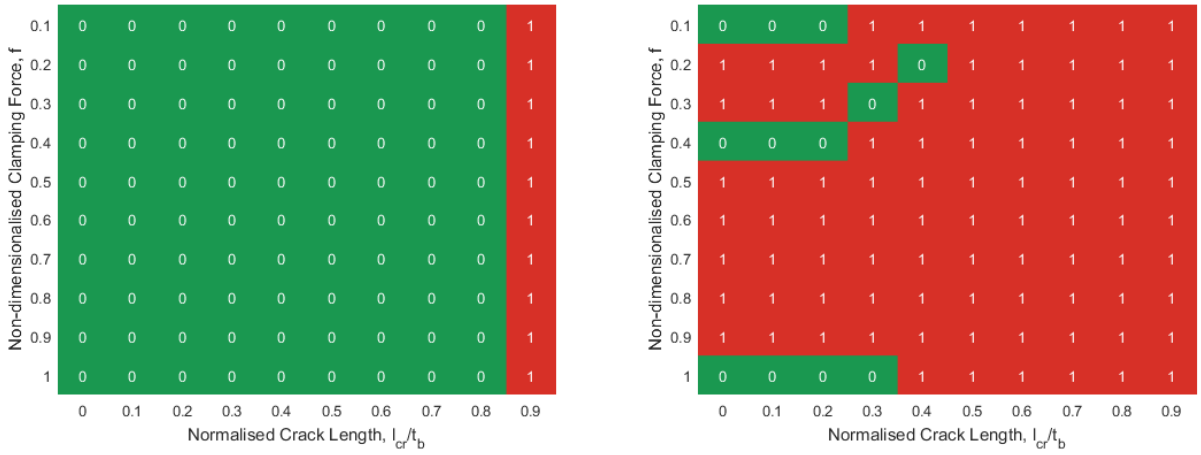

Figure 7: Kolmogorov-Smirnoff two sample hypothesis test results for the first natural frequency where both damage types are located at floor one; where (a) is the uncertainty integration strategy and (b) the original simulator.

thickness, for the uncertainty integration strategy. This indicates that the beam tip stiffness for this crack length has not accurately been captured, and should be an area of model improvement at the sub-system level. On the other hand, the original simulator fails to capture the majority of damage scenarios. It performs best when the crack length is small (under 30% of the beam thickness) and when the reduction in clamping force results in the linear model overlapping the hyperbolic tangent model (Fig. 3). Consequently, the failure to adequately capture the model form at a sub-system level will result in poor full-system performance and as all physics can never be fully captured in any model, a mechanism for quantifying the functional form and uncertainty due to model discrepancy is paramount.

To illustrate reasons for the results in Fig. 7, Fig. 5 presents a comparison of the output distributions from the 'true', original simulator and uncertainty integration strategy. The distributions are of $\Delta\omega_1$ when both damage types are located at floor one, where $f = 1$, and crack length is increased. Figure 5 shows that for $\boldsymbol{l}_{cr} = 0, 0.1, 0.2, 0.3 \times t_b$ all three distributions are overlaid with little difference in the probability mass. As the crack length increases further, a shift in the output mean of the original simulator occurs in Fig. 7, leading

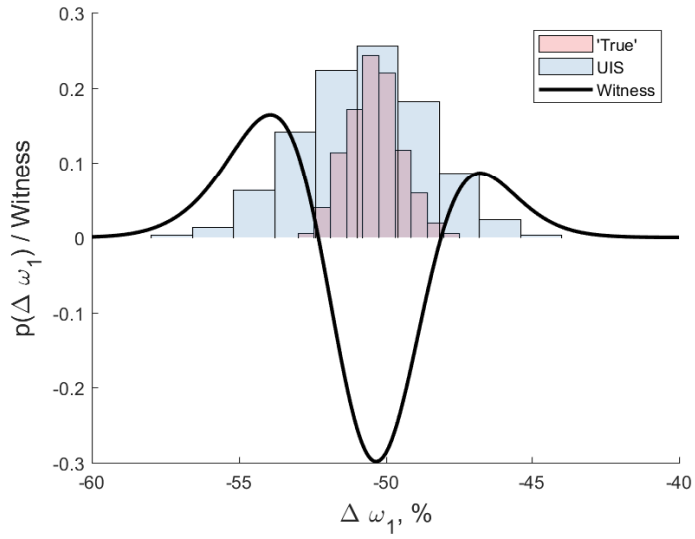

Figure 8: A comparison of the histograms and witness function of $\Delta\boldsymbol{\omega}_1$ for $l_{cr} = 0.9 \times t_b$ at floor one. UIS is the uncertainty integration strategy histogram and witness the witness function.

to a rejection in the null hypothesis. The uncertainty integration strategy provides a good fit with the 'true' full-system until $l_{cr} = 0.9 \times t_b$, where the true system has a greater variance - the percentage difference of the mean and variance at this damage extent are 0.01% and 4.69%. These differences are highlighted in Fig. 8, where the witness function, the difference between two kernel mappings of the samples [14, 15], is presented. The witness function was generated using a Gaussian kernel where the scale parameter σ, was set using a median heuristic. The witness function provides a visual illustration the offset in mean and smaller variance.

4 Conclusion

A multi-level uncertainty integration strategy based on a subfunction discrepancy approach has been demonstrated. The strategy seeks to divide a structure into different levels and sub-systems where validation of damage mechanisms is achievable. At each of these sub-systems model discrepancies are inferred in order to improve the predictive capability of the simulator. Finally, the sub-system model discrepancies and parameter uncertainties are propagated through to the full-system level providing confidence in predictions at a full-system level.

A numerical case study has been presented demonstrating the technique on a simple four degree of freedom shear structure. The objective of this study was to predict damage sensitive features - percentage differences of natural frequencies - when two types of damage were introduced to the structure, namely a midpoint crack of increasing length and a reduction in clamping force at the joint, for various positions in the structure. The full-system was divided into one level where there were two sub-systems, a beam sub-system and joint sub-system. At each of these sub-systems experimental data was generated from the 'true' process with the addition of observational uncertainty, and model discrepancies inferred between simulator outputs and the experimental data. The uncertainties and model discrepancies were propagated to the full-system level where, due to the numerical nature of the case study, a comparison was made with the 'true' outputs. Hypothesis testing was performed on the output distributions for the 6400 combinations of inputs. This demonstrated that the multi-level uncertainty strategy had improved the predictive performance from 30.7% to 97.4% of not rejecting the null hypotheses. In terms of mean predictions the strategy improved NMSEs from 104 to 0.005. The enhanced predictive capability clearly indicates the benefits of this approach for the case study.

Further research should be conducted into applying the methodology to a real world case study and for different types of simulator and model fidelities. The approach should also be applied with different divisions of a structure in order to quantify the differences in outputs due to the initial set up of the technique. Additionally, demonstration of the process with calibration included is left as further work. Finally, the inclusion of hetroscedastic Gaussian processes to better capture the model discrepancies from hetroscedastic experimental data should be pursued.

References

[1] P Gardner, C Lord, and R. J. Barthorpe. A Probabilistic Framework for Forward Model-Driven SHM. In *European Workshop on Structural Health Monitoring (EWHSM)*, pages 1–13, 2018.

[2] M. Strong, J. E. Oakley, and J. Chilcott. Managing Structural Uncertainty in Health Economic Decision Models. *Journal of the Royal Statistical Society: Series C (Applied Statistics)*, 61(1):25–45, 2012.

[3] M. C. Kennedy and A. O'Hagan. Bayesian calibration of computer models. *Journal of the Royal Statistical Society: Series B (Statistical Methodology)*, 63(3):425–464, 2001.

[4] J Brynjarsdóttir and A O'Hagan. Learning about physical parameters: the importance of model discrepancy. *Inverse Problems*, 30(11):114007, 2014.

[5] A O'Hagan and J. F. C. Kingman. Curve Fitting and Optimal Design for Prediction. *Journal of the Royal Statistical Society. Series B (Methodological)*, 40(1):1–42, 1978.

[6] C. E. Rasmussen and C. K. I. Williams. *Gaussian processes for machine learning.*, volume 14. 2004.

[7] G. E. P. Box and N. R. Draper. *Empirical Model-Building and Response Surfaces*. 1987.

[8] S. Christides and A. D. S. Barr. One-dimensional theory of cracked Bernoulli-Euler beams. *International Journal of Mechanical Sciences*, 26(11-12):639–648, 1984.

[9] J. K. Sinha, M. I. Friswell, and S Edwards. Simplified Models for the Location of Cracks in Beam Structures Using Measured Vibration Data. *Journal of Sound and Vibration*, 251(1):13–38, 2002.

[10] M Lazaro-Gredilla and M Titsias. Variational Heteroscedastic Gaussian Process Regression. *Proceedings of International Conference on Machine Learning (ICML 2011), Bellevue, Washington, USA*, page 8, 2011.

[11] M. D. Todd, J. M. Nichols, C. J. Nichols, and L. N. Virgin. An assessment of modal property effectiveness in detecting bolted joint degradation: Theory and experiment. *Journal of Sound and Vibration*, 275(3-5):1113–1126, 2004.

[12] J. M. Nichols and K. D. Murphy. *Modeling and Estimation of Structural Damage*. John Wiley & Sons, Ltd, Chichester, UK, feb 2016.

[13] P Gardner, R. J. Barthorpe, and C Lord. The Development of a Damage Model for the use in Machine Learning Driven SHM and Comparison with Conventional SHM Methods. In *Proceedings of ISMA2016 International Conference on Noise and Vibration Engineering*, pages 3333–3346, 2016.

[14] A Gretton. A Kernel Two-Sample Test. *Journal of Machine Learning Research*, 13:723–773, 2012.

[15] P Gardner, C Lord, and R. J. Barthorpe. An Evaluation of Validation Metrics for Probablistic Model Outputs. In *Proceedings of the ASME 2018 Verification and Validation Symposium*, 2018.